Journal of Power Sources 202 (2012) 28–34

Contents lists available at SciVerse ScienceDirect

Journal of Power Sources

journal homepage: www.elsevier.com/locate/jpowsour

Preparation and characterization of bifunctional graphitized carbon-supported Pt composite electrode for unitized regenerative fuel cell

Yi-Hao Pai*, Chun-Wei Tseng

Department of Opto-Electronic Engineering, National Dong Hwa University, No. 1, Sec. 2, Da Hsueh Rd., Shoufeng, Hualien 97401, Taiwan, ROC

ARTICLE INFO

Article history:
Received 11 September 2011
Received in revised form 2 November 2011
Accepted 3 November 2011
Available online 12 November 2011

Keywords:
Unitized regenerative fuel cell
Oxygen electrode
Montmorillonite
Graphitized carbon-support

ABSTRACT

A bifunctional graphitized carbon-supported Pt oxygen electrode with montmorillonite-assisted dispersion was synthesized using an ultrasonic mixed technique process. By comparison, the graphitized carbon-supports obtain the optimal crystal quality with decreasing I_D/I_G ratio from 1.43 to 0.81 and narrow the peak linewidth from 186 to 84 cm^{-1}. Both Raman and the selected area diffraction analysis illustrate that the amorphous carbon tends to decrease via high-temperature graphite annealing so that the number of active C atoms will be reduced to improve oxidation resistance. From the CV measurements, the 20 wt.% Pt/graphite produces the highest specific charge transfer due to helpful montmorillonite assisted dispersion, whereas Pt size can only aggregate to grow bigger with an increase the Pt/graphite concentration. The polarization test of URFC presents the optimal performance in both the water electrolysis and fuel cell modes, with cell potentials of 1.6 V and 0.6 V at 100 mA cm^{-2}, respectively; it exhibits an optimized energy conversion efficiency of 37.5%, which is better than a Pt/C electrocatalyst-coated membrane due to its having more mass transportation formation and corrosion suppression. By using generated hydrogen to produce electricity, the total energy transfer efficiency of the cell measurement system will reach 50.6%.

1. Introduction

Recently, there has been increased interest in developing catalyst supports for fuel cells, and the field of engineering is using different technologies to study the carbon-based supports, e.g. carbon blacks (Vulcan XC72) [1–3]. Typically, the catalyst supports must provide a high surface area for supporting the active catalyst particles as well as reducing catalyst loading. Additional roles would provide good electronic conductivity, corrosion resistance and low cost [1–4]. However, such a carbon black material is unsuitable for use in unitized regenerative fuel cells (URFC); the high potential (about 1.0 V) at the oxygen electrode during water electrolysis will lead to heavy oxidation/corrosion of carbon blacks with the oxidation rate rising along with the potential [5]. In particular, the corrosion rate will be accelerated since Pt catalysts exist on the surface of the carbon blacks; this will lead to a significant performance loss in the URFC [2]. Note that the oxidation/corrosion of the carbon black affects the electrical contact and increases cell polarization, which subsequently leads to mass transport losses and declining cell stability [1]. Some early studies have reported on the use of carbon substitutes as electrical conductors (e.g. boron carbide (B_4C) and titanium carbide (TiC)) as possible catalyst supports for use in the oxygen electrodes of URFCs [1,6,7]. Several groups have also referred to transition-metal oxides (e.g. IrO_2 or RuO_2) as possible support in catalysis for the bifunctional oxygen electrode [8,9]. Although most of these support materials may show good corrosion resistance for use in URFC, their high cost and complex processes, as demonstrated with the current noble-metal-oxide support, make them less feasible for manufacturing.

In one study, Ferreira-Aparicio et al. preliminarily demonstrated the use of high surface area graphite as an alternative support for proton exchange membrane fuel cell (PEMFC) catalysts. They suggested that the extent of the carbon support graphitization plays an important role in achieving electrochemical and thermal stability, with more graphitic carbons demonstrating increased electrocatalyst stability [10]. Not long ago, Wang et al. also reported on a nanoscale graphite-supported Pt catalyst fabrication employed to improve the rate of carbon corrosion in fuel cells [11]. They found that the improved electrocatalyst not only had high cell performance similar to that of the commercial cell but also provided much better corrosion-resistance than the commercial electrocatalyst did; it could therefore possibly replace the currently used carbon blacks. Although the experimental works emphasized improving PEM fuel cell performance by changing the heat treated prescription, the dependence between support dispersion and graphite-supported Pt catalyst activity, as well as the utility of catalyst materials, has never been previously discussed. In addition, few detailed investigations have explored the round-trip

* Corresponding author. Tel.: +886 3 8634195; fax: +886 3 8634195.
E-mail address: paiyihao@mail.ndhu.edu.tw (Y.-H. Pai).

0378-7753/$ – see front matter © 2011 Elsevier B.V. All rights reserved.
doi:10.1016/j.jpowsour.2011.11.013

energy conversion efficiency of graphite-supported Pt catalysts for URFC.

In the present study, the suitability of high surface area graphitized carbon with montmorillonite-assisted dispersion as a URFC catalyst support is investigated and compared with the use of the popular carbon black (Vulcan XC72). The relationship between montmorillonite modules and the size/displacement distribution of Pt nano-dots has been characterized. Both electroactivities and electrochemical properties were evaluated for the determination of the electrochemical surface area and catalyst utilization. Polarization measurements and round-trip energy conversion efficiency analysis were also used to evaluate the effect of graphitized carbon with montmorillonite-assisted dispersion in preparing a bifunctional oxygen electrode to improve URFC performance.

2. Experimental

2.1. Preparation of graphitized carbon-supported Pt electrocatalyst

Carbon supports purchased from the Cabot Co., Ltd. were first heat-treated at 2250 °C for 60 min in a high-temperature furnace under inert gas protection [12]. Afterwards, the ultrasonic mixed technique of graphitized carbon supports and unmodified natural montmorillonite (Cloisite® Na^+) with montmorillonite concentration of 1.5 wt.% were dispersed and prepared as catalyst supports in a procedure similar to one described in a previous study [13,14]. Using the finely dispersed graphitized carbon supports, four kinds of various Pt/graphitized carbon weight ratios of 10, 15, 20 and 30 wt.% were prepared, tested and compared for use as bifunctional oxygen electrode catalysts. By using a sonochemical mixed technique [15] with the addition of $H_2PtCl_6{\cdot}6H_2O$ as a Pt black precursor (Seedchem) on graphitized carbon supports, the loading of the Nafion solution was 5 wt.%.

2.2. Physical and electrochemical characterization of graphitized carbon-supported Pt electrocatalyst

The Raman spectra of the graphitized carbon supports were measured and compared with a Raman spectrometer using a HeNe laser (632.8 nm excitation wavelength) as the light source. Subsequently, scanning transmission electron microscopy (STEM, Hitachi H-7000) and a single-lens reflex camera (OM, Olympus) were employed to accurately characterize the Pt catalyst and dispersion of the graphitized carbon supports. The average particle size was determined by high-resolution transmission electron microscopy (HRTEM). The software package "DigitalMicrograph™ 3.6.1. by Gatan" was used to determine the average Pt particle size from the real-time HRTEM image [16,17]. Note that the supported Pt particle shape normally assumed to be spherical with a face-centered cubic structure [18]. A large number of particles (360–460) could be examined to obtain the good statistical values. In order to realize the electroactivities and electrochemical properties of the graphitized carbon-supported Pt electrocatalyst, 0.01 ml of catalyst ink was loaded onto a glassy carbon disk electrode (diameter of the active zone was 3 mm). After drying, the electrochemical properties of the physically mixed Pt/graphitized carbon catalysts were analyzed by a cyclic voltammetry (CV) technique through a CHI614D electrochemical analyzer. In order to obtain information concerning electrode activities, glassy carbon disk electrodes coated with Pt/graphitized carbon catalysts were measured in a 1 M H_2SO_4 solution with a 50 mV s^{-1} scanning rate between −0.4 and 1.2 V at room temperature, while a Pt wire served as the counter electrode and an Ag/AgCl served as the reference electrode.

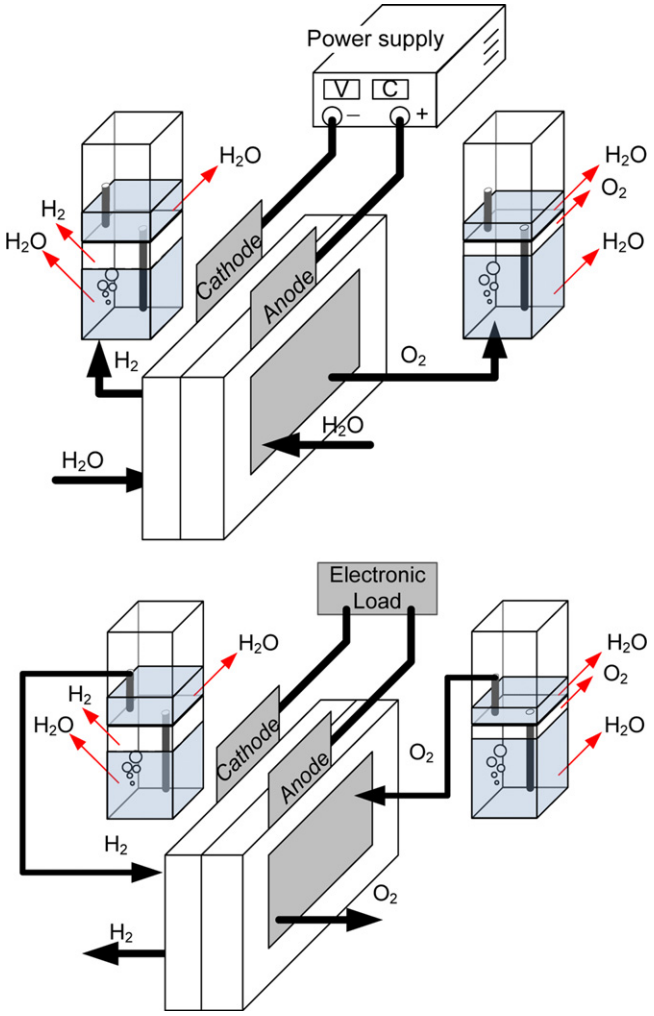

Fig. 1. Schematic operation of a URFC system, (top) PEM electrolyzer and (down) PEM fuel cell.

2.3. Bifunctional membrane electrode assembly (MEA) preparation and unit cell test

To evaluate the round-trip energy conversion efficiency and cell performance of a bifunctional MEA, the maximum charge transferred for hydrogen adsorption obtained from the CV curve of a graphitized carbon-supported Pt electrocatalyst sample was employed in the fabrication of the URFC unit cell. First, the electrocatalyst ink was coated onto both sides of a 9 cm^2 polymer electrolyte membrane (DuPont-Nafion 212), followed by drying at 70 °C. Next the polymer electrolyte membrane was interposed between the two gas diffusion layers (GDLs) using a hot pressing system; the anode/PEM/cathode module was used as the MEA in polarization measurements. Note that the catalyst loading in the electrodes was kept at a constant value of 0.25 mg cm^{-2}. In order to compare the improved performance of their round-trip energy conversion properties, we also prepared a popular carbon black- (Vulcan XC72) based MEA with the same catalyst loading and dispersion method. Subsequently, the MEA was placed in a unit cell, and the cell performance was measured via a cell measurement system; this included the URFC cell, water tanks, DC power supply and electronic loads, as shown in Fig. 1. In the electrolyzer mode, an external power source (DC power supply) provided power directly to the URFC unit cell in order to decompose the water into H_2 and O_2 according the following reaction of $2H_2O$ + electrical energy + heat → $2H_2 + O_2$. In the fuel cell mode, the

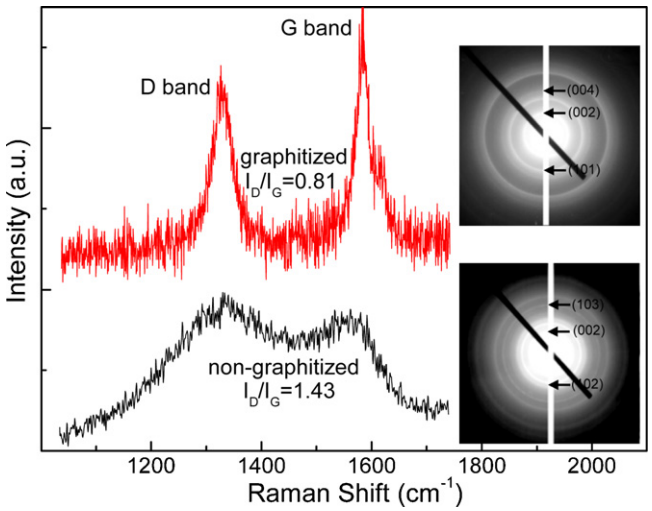

Fig. 2. Raman spectra of graphitized and non-graphitized carbon supports; (inset: SAD patterns).

reflux fuel (H_2 and O_2) was supplied to the anode and cathode, and the cell became the power source which delivered current, voltage and power into the attached resistive load according to the following reaction: $2H_2 + O_2 \rightarrow 2H_2O$ + electrical energy + heat. The performance of the URFC in the round-trip energy conversion test was evaluated by measuring the voltage transients under a constant current density of 100 mA cm^{-2}. The duration of each cycle was 14 min, with 7 min in the electrolyzer mode and 7 min in the fuel cell mode.

3. Results and discussion

3.1. Characterization of graphitized carbon supports with montmorillonite assisted dispersion

To evaluate the quality of carbon materials, the graphitization degree of the as-received and the graphitized carbon was determined using a Raman spectrometer, as shown in Fig. 2. In the Raman spectra, the first order Raman mode registered between 1300–1350 cm^{-1} and 1550–1600 cm^{-1} are constituted of D and G bands, respectively [19,20]. The D-band peak at around 1340 cm^{-1} has a high sensitivity to disorder in the graphitic sp2 network typical of carbonaceous impurities, which involves the phonons near the K Brillouin zone boundary. The G-band intensity (I_G) around 1580 cm^{-1} is ascribed to the normal graphite structure assigned to the E_{2g} phonon (vibration mode) at the Brillouin zone center [21]. Therefore, a ratio of I_D/I_G is a good indicator of the quality of carbon supports, whereas the higher ratio of I_D/I_G exhibits worse graphitization. From Fig. 2, the I_D/I_G ratio of untreated carbon supports reveals a large value of 1.43 as compared to that of treated samples, which ascribes to the defect structure inducing a large intensity of the D-band. In particular, the I_D/I_G ratio and the peak linewidth of the heat-treated carbon clearly decrease (from 1.43 to 0.81) and narrow (from 186 to 84 cm^{-1}), implying that the crystals are enhanced; they exhibit a high degree of graphitization. It is well known that the in-plane crystallite size (L_a) depends on the I_D/I_G ratio, which can be obtained through the empirical formula given by Knight, $L_a = C \times (I_D/I_G)^{-1}$, where the factor C has a notable relationship with the laser wavelength. For a 632.8 nm laser beam, the factor C is 8.28 nm [22,23]. The in-plane crystallite size of treated carbon supports estimated from the above equation is 10.22 nm; this is slightly lower than those in previous reports in several studies [12,24] and implies a relatively high surface area. The results further underlined that the graphitized carbon had become more hydrophobic compared to the original carbon supports, strongly suggesting that the graphitic supports provide more lower mass transfer than does popular carbon black (XC72) in restraining the corrosion of graphitized carbon supports [12].

The inset in Fig. 2 shows selected area diffraction (SAD) images of two of the carbon supports used in the present study. Most of the diffraction rings for the graphitic carbon supports are indexed as hexagonal graphite (JCPDS card No. 41-1487); they correspond to the (0 0 2), (1 0 1) and (0 0 4) crystal plane. The main growths of hexagonal graphite are [0 0 2] directional with corresponding lattice spacing of 3.4 Å. In comparison to the graphitic carbon supports, the untreated carbon supports clearly present a diffuse halo ring, vaguely corresponding to the (0 0 2), (1 0 2) and (1 0 3) crystal plane either due to the specimen violating the Bragg condition or to the presence of amorphous regions. Accordingly, it illustrates that the amorphous carbon tends to decrease as a result of high-temperature graphite annealing, so that the number of active C atoms will be reduced to improve oxidation resistance [25].

The morphology of catalytic supports, including popular carbon supports without dispersion agents and graphitized carbon-supports with montmorillonite-assisted dispersion, were first examined using an SEM instrument. As can be seen in Fig. 3a (left), the control experiment with popular carbon supports shows a serious aggregation phenomenon. It appears that the carbon powder easily aggregates from the pristine structure of an irregular spherical shape with an average diameter of 70–250 nm. This can be attributed to the van der Waals attraction among nanoparticles causing the aggregation. Note that the graphitized carbon supports must be dispersed because graphitized carbon particles naturally form agglomerated particles due to the strong van der Waals attraction; this limits their use [13,14]. The formed precipitates can actually even be easily perceived with the naked eye (see Fig. 3a inset). According to the literature, this interaction could be chemically modified to achieve improvement. Nevertheless, electrical conductivity and atomic structural perfection will suffer as a result of using this method [13,26]. Employing a polymer or surfactant as a dispersing aid is another practicable way to disperse graphitic carbon in solvent [27,28], but the mechanical and physical properties of the catalyst inks may be relatively weakened. In particular, by using pristine popular carbon supports to prepare the electrocatalyst, active catalyst particles will not uniformly disperse on the catalyst support, and active catalyst particles will easily aggregate. This result is illustrated in Fig. 3a (right). Such a phenomenon has also occurred in graphitic carbon supports. Pai et al. reported on the clay-assisted dispersion of carbon-based materials in a co-solvent [29]. This report indicated that clay–carbon synergy might make these composites better suited for PEM fuel cell applications; this conclusion was similar to Liu and Grunlan's report [13]. Such results are also presented in Fig. 3b (left), followed by results attained by introducing a montmorillonite. The dispersion of graphitic carbon supports is very effective in the presence of montmorillonite with an average particle size of about 10–20 nm. Simultaneously, the STEM studies confirm the fine dispersion of Pt catalyst with an average particle diameter of about 3.5 nm (Fig. 3b (right)). Furthermore, a PEMFC performance comparison between the electrodes with and without the assistance of montmorillonite is shown in Fig. 4. It is found that the electrodes with the assistance of montmorillonite show the widest ohmic polarization in single cell testing, which is larger than another condition. In particular, the electrode with the assistance of montmorillonite presents an optimal power output of 240 mW cm^{-2} with a current density of 690 mA cm^{-2}. The values are greater than this of the electrode without montmorillonite case (180 mW cm^{-2}, 500 mA cm^{-2}). According to the literature, an appropriate addition of montmorillonite not only enhances the fine dispersion of Pt catalyst but also improves wettability and hydrophilic property of anode [29].

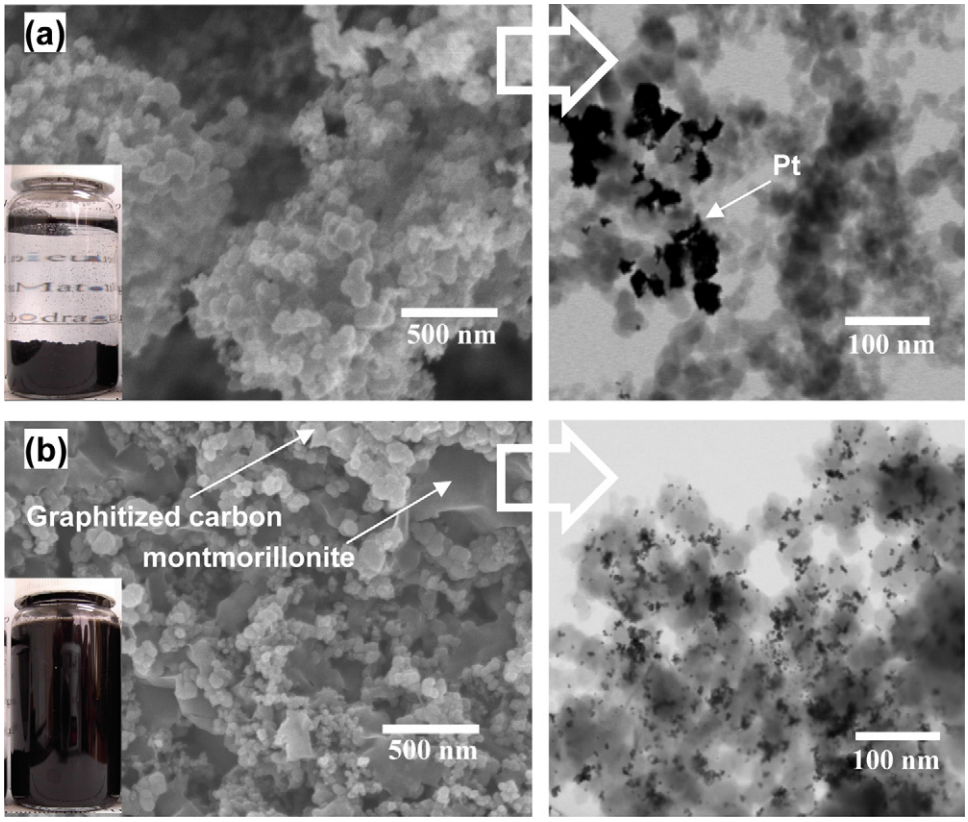

Fig. 3. FE-SEM (left) and STEM (right) micrograph of the electrocatalyst (a) commercial carbon black without dispersion agent; (b) graphitized carbon with montmorillonite dispersion agent (inset: photo images of the ink consisted of co-solvent).

3.2. Electrochemistry of graphitized carbon-supported Pt oxygen electrode

In order to further explore the dependence between Pt/graphite weight ratio and the electrochemically active surface area, CV analyses of the charge transfer reactions of various Pt/graphite weight ratios on glassy carbon electrodes were carried out, as shown in Fig. 5. It can be seen that the active specific surface area of the Pt/graphite electrocatalyst was well-defined in an H_2SO_4 medium, which involves the H-desorption and H-adsorption region around potential −0.4 to 0.05 V, the Pt-Oxide reduction peak from potential 0.2 to 0.75 V and Pt-Oxide formation peak from 0.75 to 1.2 V. The electrochemically active surface area (S_{act}) of various weight ratio samples can be calculated through the following formula: $S_{act}(cm^2\,mg^{-1}) = Q_H/Q_H^0$, where Q_H^0 is the charge of Pt with monolayer adsorption of H_2 ($210\,\mu C\,cm^{-2}$) [30]. The Q_H is the area of specific charge transfer due to hydrogen adsorption and desorption. Note that the Q_H can be obtained by the equation of $Q_H = 0.5(Q_T - Q_{DL})$. Where Q_T is the total specific charge transfer in the hydrogen adsorption/desorption potential region, which can be obtained by integration of the CV curves $\left(Q_T = (1/V)\int_{-0.4}^{0.05}(I_{desorption} - I_{adsorption})dE\right)$ in the relevant

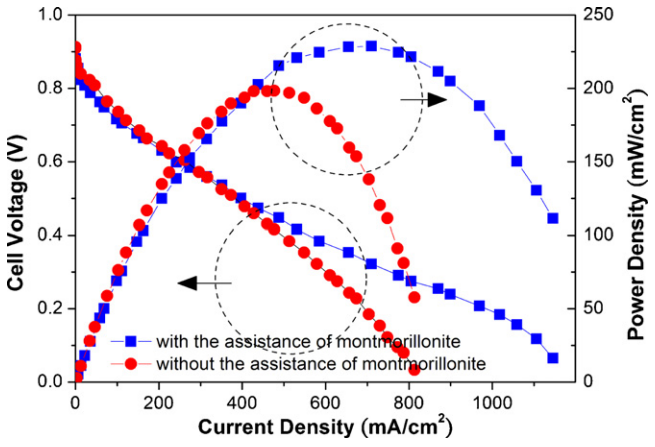

Fig. 4. Cell voltage vs. current density curves and power density vs. current density curves of electrodes with and without the assistance of montmorillonite for PEMFC testing.

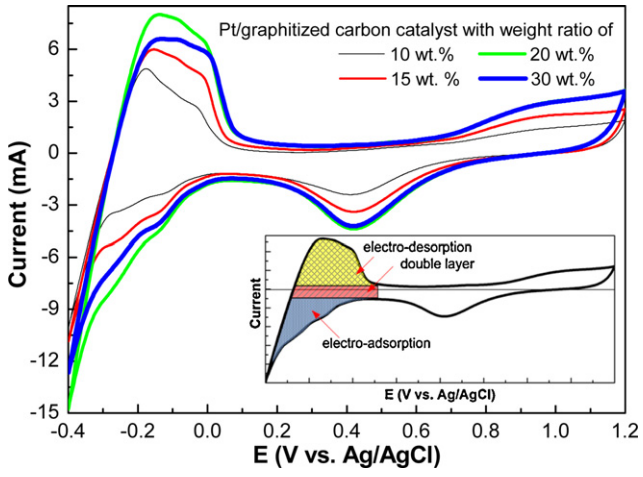

Fig. 5. Cyclic voltammograms (at $50\,mV\,s^{-1}$, in 1 M H_2SO_4 aqueous solution) of Pt/graphitized carbon electrodes with weight ratio of 10 wt.%, 15 wt.%, 20 wt.% and 30 wt.%, respectively (inset: schematic of the cyclic voltammograms curve).

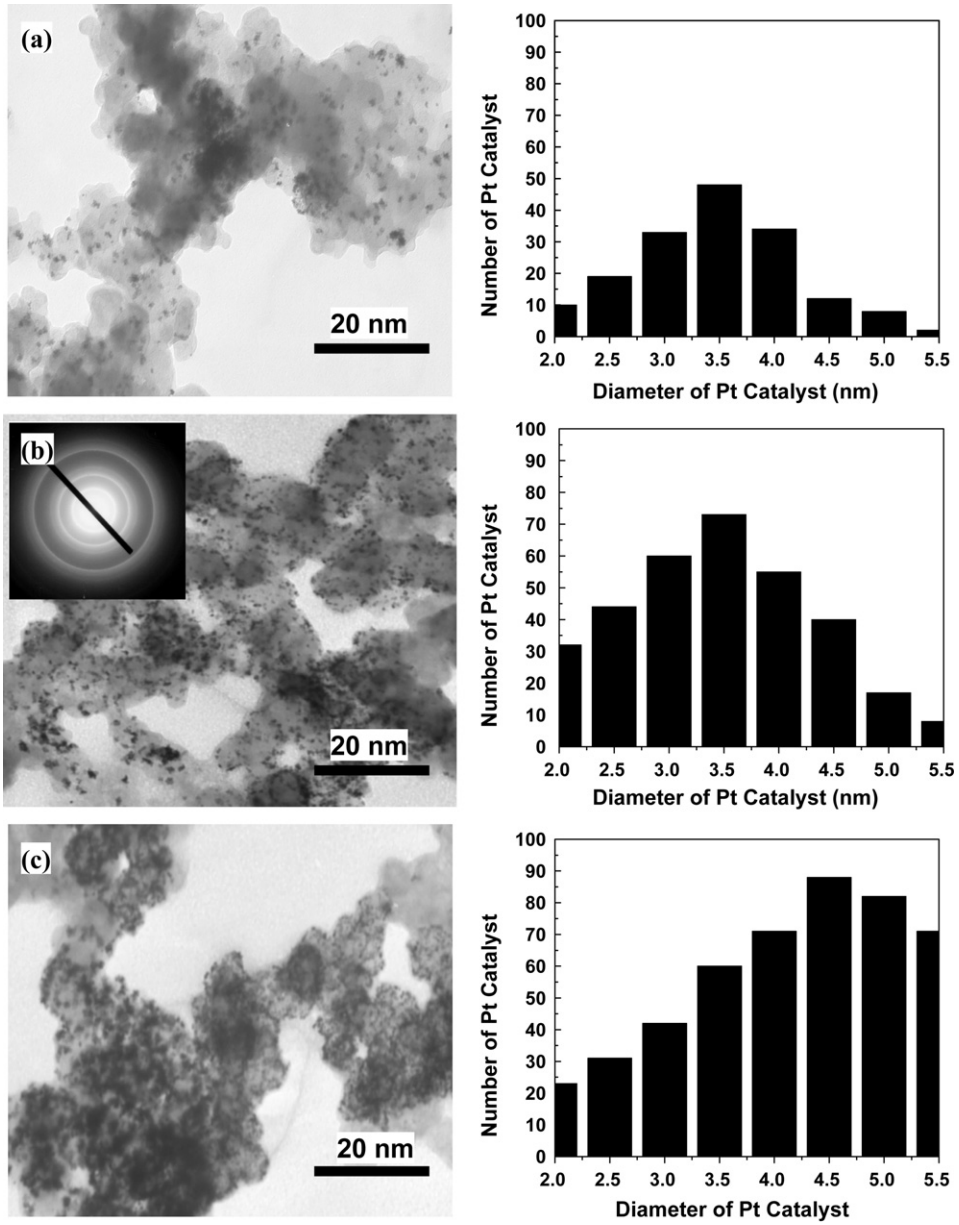

Fig. 6. TEM micrograph (left) and Pt size (right) distribution of electrocatalyst with weight ratio of (a) 10 wt.%, (b) 20 wt.%, and (c) 30 wt.%, respectively.

potential region [30]. The Q_{DL} is the specific capacitive charge in the double layers, which can also be obtained by integrating the double layer charging region. E and V are the potential and the scan rate, respectively. From the CV curves, the calculated active surface areas for the Pt/graphite weight ratios 10, 15, 20 and 30 wt.% are 381.9, 421.6, 495.2 and 457.8 $cm^2\ mg^{-1}$, respectively. In comparison, the 20 wt.% Pt/graphite produces the highest specific charge transfer in the H-desorption and H-adsorption regions; this is larger than the other Pt/graphite concentrations. This result implies that the specific charge transfer of the surface sites available for a 1.5 wt.% montmorillonite-assisted dispersion electrocatalyst with weight ratio of 20 wt.% has reached saturation.

To realize the reason for the difference in active surface areas and the utility of graphite-supported Pt catalysts, TEM images were employed to accurately characterize the Pt/graphite electrocatalyst, as shown in Fig. 6 left. In bright field images, the Pt and graphite particles appear in different contrast levels in the TEM microstructure. It is expected that the high-Z region (i.e., high mass region) may scatter more than the low-Z region of a given sample with a consistent thickness throughout. Therefore, the Pt region or high-Z region on the specimen exhibits a higher contrast, and vice versa for the graphite particles. As can be seen, the Pt active catalyst particles are very small and highly dispersed on the graphitized carbon-supports. The Pt particle size can be seen to clearly increase when the Pt/graphite weight ratio is enhanced. The average particle diameters were 3.48 ± 0.12, 3.62 ± 0.16 and 4.16 ± 0.25 nm for the 10, 20 and 30 wt.% electrocatalyst, respectively (Fig. 6 right). This result also suggests that the Pt size can only aggregate to grow bigger with an increase the Pt/graphite concentration since the number densities of Pt located sites on the graphite dispersed from ultrasonic technique are the same.

To quantify the utility of the Pt catalyst, the ratio of S_{act} and geometrical specific surface area of Pt (S_g) should be defined in order to determine how many surface atoms are active in an electrochemical reaction. Thus, assuming that all particles are spherical in shape, this ratio can be calculated using the following formula: $S_g = 6/(\rho\phi)$, where ρ is the density of Pt ($21.45\ g\,cm^{-3}$) and ϕ is the average diameter [30,31]. It can be calculated that the Pt utilization of the

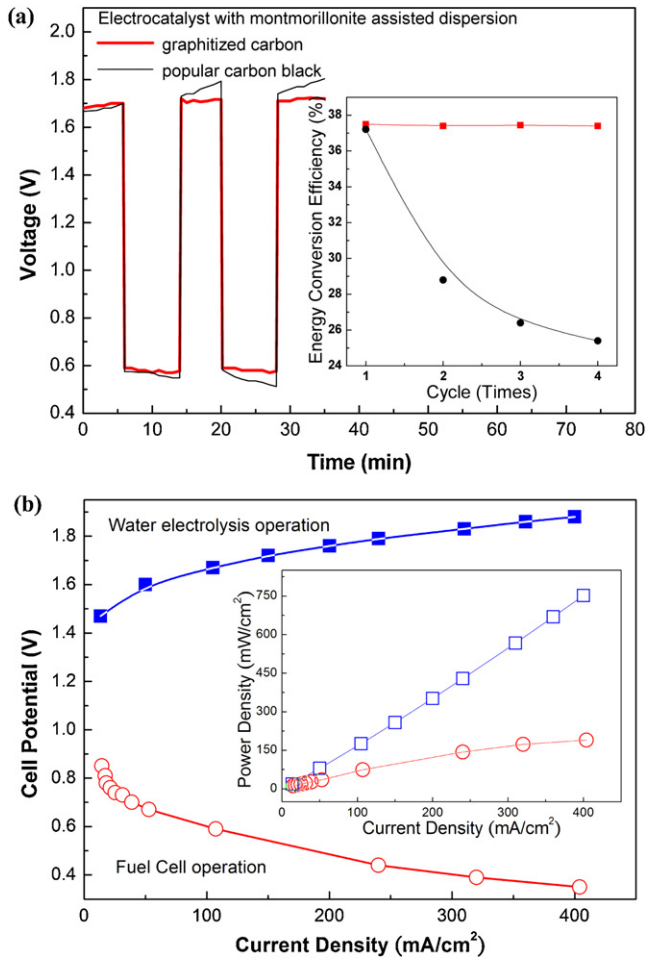

Fig. 7. (a) The cycling stability test, and (b) cell voltage vs. current density curves of MEA prepared with montmorillonite dispersion agent for weight ratio of 20 wt.% and loading of 0.25 mg cm^{-2} (inset: power density vs. current density curves).

Pt/graphite weight ratios 10, 20 and 30 wt.% are 47.5%, 64% and 68%, respectively. This is a significant finding since the Pt/graphite concentration increases by 10% (from 20 wt.% to 30 wt.%); utilization does not increase linearly (only 4%), whereas the Pt utilization is obviously enhanced 16.5% with the Pt/graphite concentration increasing from 10 to 20 wt.%. Although the electrocatalyst with 30 wt.% loading possessed higher Pt utilization than the other two Pt/graphite concentrations (e.g. 20 and 10 wt.%), it is not feasible to use Pt/graphite concentration of 30 wt.% since linearly raising Pt/graphite concentration cannot effectively and linearly enhance Pt utilization but increase the cost instead.

3.3. Round-trip energy conversion efficiency and cell performance of graphitized carbon-supported Pt for URFC

Two kinds of bifunctional oxygen electrodes with Pt/supports concentration of 20 wt.% and loading of 0.25 mg cm^{-2} coatings, including graphitized carbon and popular carbon supported Pt with montmorillonite-assisted dispersion, were prepared and compared in terms of round-trip energy conversion efficiency (7 min of electrolyzer and 7 min of fuel cell mode each), as shown in Fig. 7a. The results indicate that the graphitized carbon-supported Pt with montmorillonite-assisted dispersion had a slight performance loss: the cell voltage only dropped from 0.59 to 0.585 V throughout the period of study. The detailed *I–V* curves of URFC with the graphitized carbon-supported Pt prepared are shown in Fig. 7b. The cell voltage for water electrolysis mode was only 1.67 V at 100 mA cm^{-2} and 1.8 V at 300 mA cm^{-2}. In the fuel cell mode, the URFC shows an optimal power output of 190 mW cm^{-2} with a current density of 404 mA cm^{-2}. However, cycle performance of the popular carbon-supported Pt with montmorillonite-assisted dispersion shows obvious degradation in both water electrolysis and fuel cell operation. It did not even work for more than 3 cycles. The initial energy conversion efficiency of the round-trip operation determined from literature reports [32] is about 37.2% at 100 mA cm^{-2}, which is slightly lower than the efficiency of graphitized carbon supported Pt (37.5%). In particular, the energy conversion seriously dropped by up to 28% after only 2 cycles due to the relatively unstable mass transportation and corrosion effects. A similar phenomenon was also observed in related literature when catalyst supports without graphitization were used as the oxygen electrode [10,11].

In addition, the hydrogen production rate of the URFC using graphitized carbon-supported Pt prepared in the electrolyzer mode was about 0.34 ml min^{-1} at a current density of 105 mA cm^{-2}. The value is clearly greater than that of a URFC with popular carbon-supported Pt designed (0.23 ml min^{-1}) to provide the same current density. On the other hand, when using the generated hydrogen to produce electricity, total energy transfer efficiency (defined as electrical energy output divided by unit of energy generated from hydrogen) of the cell measurement system may reach 50.6%. Note that the hydrogen consumption was determined by the volume of water displaced during the output of electrical energy or fuel cell operation.

4. Conclusions

A bifunctional graphitized carbon-supported Pt oxygen electrode with montmorillonite assisted dispersion for unitized regenerative fuel cell was demonstrated. Characterizations of the electrocatalyst supports from Raman reveal enhanced crystal properties of graphitized carbon-supports with decreasing I_D/I_G ratio from 1.43 to 0.81 and narrow the peak linewidth from 186 to 84 cm^{-1}. By utilizing the 1.5 wt.% montmorillonite assisted dispersion, the fine Pt/graphite electrocatalyst can be obtained with an average particle diameter of about 3.5 nm. The optima Pt/graphite weight ratio and utilization are 20 wt.% and 64%, whereas the Pt/graphite concentration increases by 10% (from 20 wt.% to 30 wt.%), but utilization does not increase linearly (only 4%). Such an electrocatalyst provides a more stable and corrosion-resistant in round-trip operation and exhibits an optimized energy conversion efficiency of 37.5%. Simultaneously, the evaluated hydrogen production rate of the URFC in the electrolyzer mode was about 0.34 ml min^{-1} at a current density of 105 mA cm^{-2}. By using the generated hydrogen to produce electricity, total energy transfer efficiency of the cell measurement system may reach 50.6%.

Acknowledgements

This work was supported in part by the National Science Council (NSC) of the Republic of China, under grants NSC 100-2218-E-259-001 and NSC 99-2218-E-259-002.

References

[1] J. Pettersson, B. Ramsey, D. Harrison, J. Power Sources 157 (2006) 28.
[2] H. Tang, Z. Qi, M. Ramani, J.F. Elter, J. Power Sources 158 (2006) 1306.
[3] E. Antolini, Appl. Catal. B: Environ. 88 (2009) 1.
[4] C.-H. Wang, H.-Y. Du, Y.-T. Tsai, C.-P. Chen, C.-J. Huang, L.C. Chen, K.H. Chen, H.-C. Shih, J. Power Sources 171 (2007) 55.
[5] X.Z. Yuan, H. Li, S. Zhang, J. Martin, H. Wang, J. Power Sources 196 (2011) 9107.
[6] W.T. Grubb, D.W. Mckee, Nature (London) 210 (1966) 192.
[7] G. Chen, S.R. Bare, T.E. Mallouka, J. Electrochem. Soc. 149 (8) (2002) A1092.
[8] T. Ioroi, K. Yasuda, Z. Siroma, N. Fujiwara, Y. Miyazaki, J. Power Sources 112 (2002) 583.

[9] G. Chen, D.A. Delafuente, S. Sarangapani, T.E. Mallouk, Catal. Today 67 (2001) 341.
[10] P. Ferreira-Aparicio, M.A. Folgado, L. Dazaa, J. Power Sources 192 (2009) 57.
[11] M. Wang, F. Xu, H. Sun, Q. Liu, K. Artyushkova, E.A. Stach, J. Xie, Electrochim. Acta 56 (2011) 2566.
[12] C.C. Hung, P.Y. Lim, J.R. Chen, H.C. Shih, J. Power Sources 196 (2011) 140.
[13] L. Liu, J.C. Grunlan, Adv. Funct. Mater. 17 (2007) 2343.
[14] M.S. Strano, Nat. Mater. 5 (2006) 433.
[15] Y. Han, S. Li, X. Wang, I. Bauer, M. Yin, Ultrason. Sonochem. 14 (2007) 286.
[16] J. Garcia-Martinez, N. Linares, S. Sinibaldi, E. Coronado, A. Ribera, Micropor. Mesopor. Mater. 117 (2009) 170.
[17] Y. Ji, A.M.J. van der Eerdena, V. Koot, P.J. Kooyman, J.D. Meeldijk, B.M. Weckhuysen, D.C. Koningsberger, J. Catal. 234 (2005) 376.
[18] C.R. Adams, H.A. Benesi, R.M. Curtis, R.G. Meisenheimer, J. Catal. 1 (1962) 336.
[19] A. Jorio, M.A. Pimenta, A.G. Souza Filho, R. Saito, G. Dresselhaus, M.S. Dresselhaus, New J. Phys. 5 (2003) 139.1.
[20] S. Reich, C. Thomsen, J. Maultzsch, Carbon Nanotubes: Basic Concepts and Physical Properties, John Wiley & Sons, Berlin, Germany, 2004.
[21] D. Mattia, M.P. Rossi, B.M. Kim, G. Korneva, H.H. Bau, Y. Gogotsi, J. Phys. Chem. B 110 (2006) 9850.
[22] M.J. Matthews, M.A. Pimenta, G. Dresselhaus, M.S. Dresselhaus, M. Endo, Phys. Rev. B 59 (10) (1999) R6585.
[23] F.C. Tai, C. Wei, S.H. Chang, W.S. Chen, J. Raman Spectrosc. 41 (2010) 933.
[24] Y. Zhang, Y.H. Tang, L.W. Lin, E.L. Zhang, Trans. Nonferrous Met. Soc. China 18 (2008) 1094.
[25] A. Chambers, T. Nemes, N.M. Rodriguez, R.T.K. Baker, J. Phys. Chem. B 102 (12) (1998) 2251.
[26] H. Park, J. Zhao, J.P. Lu, Nano Lett. 6 (2006) 916.
[27] J.C. Grunlan, L. Liu, Y.S. Kim, Nano Lett. 6 (2006) 911.
[28] T. Chatterjee, K. Yurekli, V.G. Hadjiev, R. Krishnamoorti, Adv. Funct. Mater. 15 (2005) 1832.
[29] Y.H. Pai, J.H. Ke, C.C. Chou, J.J. Lin, J.M. Zen, F.S. Shieu, J. Power Sources 163 (2006) 398.
[30] Y. Xing, J. Phys. Chem. B 108 (2004) 19255.
[31] Y. Shao, G. Yin, J. Wang, Y. Gao, P. Shi, J. Power Sources 161 (2006) 47.
[32] T. Ioro, T. Oku, K. Yasuda, N. Kumagai, Y. Miyazaki, J. Power Sources 124 (2003) 385.